ACS Catalysis

Research Article

pubs.acs.org/acscatalysis

Propylene Hydrogenation and Propane Dehydrogenation by a Single-Site Zn^{2+} on Silica Catalyst

Neil M. Schweitzer,[†,⊥] Bo Hu,[†,§] Ujjal Das,[†] Hacksung Kim,[†,‡] Jeffrey Greeley,[†,∥] Larry A. Curtiss,[†] Peter C. Stair,[†,‡] Jeffrey T. Miller,*[,†] and Adam S. Hock*[,†,§]

[†]Argonne National Laboratory, Argonne, Illinois 60439, United States

[‡]Northwestern University, Evanston, Illinois 60208, United States

[§]Illinois Institute of Technology, Chicago, Illinois 60616, United States

ABSTRACT: This study reports the highly selective (more than 95%) dehydrogenation of propane to propylene as well as the reverse hydrogenation reaction by silica-supported single-site Zn(II) catalyst. The catalyst is thermally stable at dehydrogenation temperature (550 °C and above), and catalytic byproducts are small. In situ UV-resonance Raman, XANES, and EXAFS spectra reveal that tetrahedrally coordinated Zn(II) ions are chemisorbed into the strained three-membered siloxane rings on the amorphous silica surface. Under reaction conditions, the Zn(II) ion loses one Zn−O bond, resulting in a coordinatively unsaturated, 3-coordinate active center. The infrared spectrum of adsorbed pyridine indicates that these are Lewis acid sites. Theoretical calculations based on hybrid density functional theory suggest that the catalyst activates H−H and C−H bonds by a nonredox (metal) mechanism consisting of heterolytic cleavage of C−H bonds, in contrast with the homolytic mechanisms such as oxidative addition/reductive elimination pathways. The computed minority catalytic pathway consists of undesired C−C bond cleavage at Zn(II) site, follows a slightly different mechanism, and has a significantly higher activation energy barrier. These mechanisms are consistent with the high olefin selectivity observed for single-site Zn(II) on SiO_2.

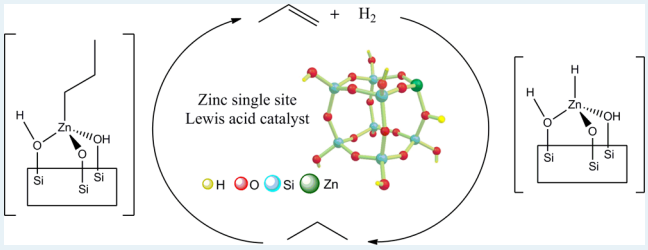

KEYWORDS: *single-site catalysts, propane dehydrogenation, propylene hydrogenation, heterogeneous Zn catalysis, Lewis Acid hydrogenation/dehydrogenation catalysis*

1. INTRODUCTION

As global demand for hydrocarbon reserves has continued to increase, more efficient utilization of these resources has become an important and complementary strategy to the development and deployment of sustainable energy generation. Olefin production is critical to the polymer and chemical industries as well as for the production of fuels. Currently, olefins are produced by thermal cracking[1] or by catalytic dehydrogenation of alkanes using supported Pt metal or Cr oxide[2] catalysts. Both processes operate at high temperatures above 450 °C, where thermodynamics favors high olefin yields. For alkanes with three or more carbons, all the current processes result in mixtures of C−C and C−H cracked products. For example, propane thermal cracking produces propylene, ethylene, methane, and hydrogen. Because of lower propylene selectivity associated with thermal cracking, catalytic processes are favored with propane. Although higher propylene selectivity is generally attained, catalyst deactivation due to the deposition of carbon on the catalyst surface is often severe, requiring frequent or continuous catalyst regeneration. Therefore, further improvements in the propylene selectivity, that is, reducing the C−C cleavage reaction, remains an important catalytic goal.

ZnO is weakly active for the catalytic hydrogenation of olefins[3] at room temperature but becomes active after high-temperature treatment. Bulk ZnO has been shown to activate hydrogen, hydocarbons, and olefins through a heterolytic cleavage mechanism. The active site has been proposed to be a defect site formed by dehydration of two adjacent Zn−OH groups at elevated temperatures to evolve H_2O and form a Zn−O−Zn site. Hydrogen was thought to dissociate on the low coordinate Zn(II) ions, forming Zn−H and a Zn−OH sites in a stoichiometric manner. ZnO was not active for the dehydrogenation of alkanes. At high temperatures, it reduces to form zinc metal, which is a liquid (mp 420 °C[4]) around the temperatures where dehydrogenation becomes favorable. Thus, hydrogenation is possible over ZnO, but dehydrogenation is not, because of the instability of ZnO at high temperatures.

Alternatively, single-site Zn(II) ions in MFI zeolite have often been suggested to catalyze alkane dehydrogenation during conversion of propane to aromatics.[5] Although Zn(II) and Ga(III)[6] ions improve the catalyst performance, Brönsted sites in these catalysts also promote these same reactions.[7] In

Received: November 25, 2013
Revised: February 17, 2014
Published: February 21, 2014

addition, because the initially formed olefins rapidly react at the Brönsted sites, undergoing oligomerization, isomerization, cracking, and aromatization, it has not been possible to demonstrate the independent catalytic function of these exchanged cations. Attempts have been made to neutralize the acid sites, but residual protons contribute significantly to the observed catalysis.[5a] Nevertheless, Zn^{2+} ions have been suggested to catalytically dehydrogenate alkanes to olefins.

The hydrogenation reactivity of ZnO and the catalytic properties Zn/MFI suggest that low-coordinate, single-site Zn^{2+} may be capable of dehydrogenating alkanes to olefin and hydrogen catalysis if it can be stabilized toward reduction; however, the coordination geometry of the Zn^{2+} site is a key parameter for catalytic activity. For example, Zn^{2+} is bound ionically to H-MFI catalysts, forming a 6-coordinate ion pair in the presence of water.[5a] The impact of more covalent ligand/support interactions has not been reported, although it is reasonable to believe that Zn^{2+} could be an active and selective dehydrogenation catalyst *if isolated in the correct ligand environment* on a solid support.

In this paper, we report the synthesis of a silica-supported, single-site Zn(II) catalyst that is catalytically active for propylene hydrogenation and highly selective for the reverse reaction of propane dehydrogenation to propene and hydrogen. Raman spectroscopy indicates that the Zn(II) cation selectively reacts with 3-membered siloxane rings on silica to stabilize the single site structure. Using in situ X-ray absorption spectroscopy (XAS), the initial coordination geometry was found to have four Zn−O bonds. Under reaction conditions, there is loss of one Zn−O bond, giving 3-coordinate Zn site that is the unsaturated, active zinc site without a change in the Zn(II) oxidation state. Infrared spectroscopy of adsorbed pyridine shows these are Lewis acid sites. The catalyst is readily poisoned by Lewis bases, with the loss of one active site per adsorbed poison, suggesting that nearly every Zn(II) is equally active.

On the basis of density functional theory calculations, a reaction pathway for olefin hydrogenation and alkane dehydrogenation is proposed. A key step in the pathway is the reaction of 3-coordinate Zn(II) to heterolytically dissociate C−H sigma bonds in alkane dehydrogenation and H−H sigma bonds in olefin hydrogenation, followed by rate-determining β hydride elimination of the resulting Zn(II) propyl (for the dehydrogenation reaction). The relative ease of the C−H and H−H heterolytic dissociation versus C−C dissociation is the reason for the high observed selectivity in the propane dehydrogenation reaction.

2. EXPERIMENTAL SECTION

Catalyst Synthesis. The Zn/SiO_2 catalyst was synthesized using the strong electrostatic adsorption methodology.[8] Twenty-five grams of silica (SiO_2, Davisil 646, 35−60 mesh, 300 m^2/g and 1.1 cc/g, Aldrich) was suspended in ∼200 mL of deionized water. The pH of the solution was adjusted to 11 using concentrated ammonium hydroxide (NH_4OH). In a separate flask, 5 g of zinc nitrate hexahydrate ($Zn(NO_3)_2 \cdot 6H_2O$, Aldrich), which is in excess of one monolayer of adsorbed precursor on the support surface, was dissolved in 50 mL of deionized water and adjusted to a pH of 11 using ammonium hydroxide. Initially, the Zn solution precipitated, but continued addition of NH_4OH resulted in a clear, colorless solution. The basic Zn solution was rapidly added to the silica, and the solution was stirred for 10 min. After the solid was allowed to settle for 5 min, the solution was decanted. The resultant slurry was rinsed by adding 200 mL of H_2O and stirring for 10 min. After the solid settled, the water was decanted. The resulting slurry was vacuum filtered, rinsed several times with deionized water, dried overnight in air at 125 °C, and subsequently calcined in air with a 1 h ramp to 300 °C and maintained for 3 h. The Zn loading was determined to be 3.9% by Galbraith Laboratories, Inc. (Knoxville, TN) using inductively coupled plasma atomic emission spectroscopy.

Catalyst Testing Procedures. The catalyst performance testing was conducted in a vertical, quartz tube reactor equipped with mass flow controllers. The products were determined by online gas chromatography (50 m GS-Alumina capillary column). In a typical test, ∼1 g (3.5 cc) of catalyst was supported on quartz wool with an internal thermal couple positioned at the top of the catalyst bed. Initially, the catalyst was purged with He (99.999%, Airgas USA, LLC), which had been further purified using an oxygen trap, at 300 mL/min at room temperature and then for 15 min at about 100 °C. Then the temperature of the reactor was raised to the reaction temperature (200 °C for hydrogenation, 550 or 650 °C for dehydrogenation) and given 2−3 h for the temperature to stabilize. Once the temperature had stabilized, He was changed to the reactant stream. For propylene hydrogenation, the reaction mixture was 88 mL/min of 4% H_2/Ar mixture and 16 mL/min 4% propene/Ar, resulting in a contact time of ∼2.0 s. For propane dehydrogenation, the reaction mixture was 3% propane/Ar at 55 mL/min, giving a contact time of 3.8 s. Generally, the conversions were under differential conditions, that is, <10%; however, the flow rate and temperature were also varied to obtain higher conversions. Product composition was determined by gas calibration standards and analyzed by a flame ionization detector (FID) using H_2 (99.999%, Airgas USA, LLC) and air (<2 ppm H_2O, Airgas USA, LLC).

Catalyst poisoning experiments were conducted by loading the catalyst into a round-bottom flask sealed with a septum. The flask was then attached to a Schlenk line, at <2 Torr pressure, and heated to 160 °C. After evacuation and without opening to air, a predetermined amount of isopropyl alcohol or pyridine was injected via syringe into the flask through the septum, where it vaporized and adsorbed to the catalyst surface over 1 h. The catalyst was then loaded into the quartz reactor tube (in air) and tested as described above. The 0.25 and 0.5 equivalents were 2-propanol-poisoned, and pyridine was used for the 1.0 equivalents. The pyridine sample was also used for infrared study before and after catalysis (see below).

In Situ X-ray Absorption (XAS) Experiments. Measurements of the Zn K-edge (9.659 keV) were conducted on the bending magnet beamline of the Materials Research Collaborative Access Team (MRCAT, 10-BM) at the Advanced Photon Source (APS), Argonne National Laboratory. The catalyst was pressed into a 4 mm self-supporting wafer and placed in a stainless steel holder. The holder was then placed into a quartz tube (1 in. o.d., 10 in. length) reactor capped with Ultra-Torr fittings equipped with shut-off valves. Both ends of the reactor were sealed with Kapton windows. The reactor contains an internal thermocouple, located at the sample, that controls the clam shell furnace.[9] The catalyst was tested at room temperature after synthesis, in flowing H_2/propylene/He (100 cc/min) at 200 °C and propane/He at 550 °C for the corresponding XANES data. To minimize contributions due to thermal effects, after the XAS measurements at elevated temperature, the data were also obtained after the catalysts

dx.doi.org/10.1021/cs401116p | ACS Catal. 2014, 4, 1091−1098

were cooled in He to room temperature without exposure to air.

Ionization chambers were optimized at the midpoint of the Zn spectrum for the maximum current with linear response (~10^{10} photons detected s^{-1}) using 5% Ar in N_2 (15% absorption) in the incident X-ray detector and a mixture of ~25% Ar in N_2 (70% absorption) in the transmission X-ray detector. A third detector in the series simultaneously collected a Zn foil reference spectrum with each measurement for energy calibration. A cryogenically cooled double-crystal Si(111) monochromator was used and detuned to 50% to minimize the presence of harmonics. The X-ray beam was 0.5 × 1.5 mm, and data were collected in transmission geometry over 10 min in step-scan mode.

The Zn K-edge XANES energy was determined from the inflection point of the leading edge by determination of the energy of the maximum in the first peak of the first derivative. Extended X-ray absorption fine structure (EXAFS) fits of the Zn/silica catalysts were determined from experimental phase shift and backscattering amplitudes, which were obtained from the ZnO (3 Zn−O at 1.97 Å and 1 Zn−O at 1.99 Å[10]). Standard procedures based on WINXAS 3.1 software were used to fit the XAS data. The EXAFS coordination parameters were obtained by a least-squares fit in r-space of the first shell nearest neighbor, k^2-weighted Fourier transform data.

Raman Spectroscopy. The excitation wavelength of 287 nm for in situ UV Raman measurements are provided by third-harmonic generation output of a 4 kHz repetition rate, nanosecond-pulsed, wavelength-tunable Ti:sapphire laser (Coherent, Indigo-S).[11] The laser power delivered to the catalyst was 3 mW. UV Raman spectra were recorded with a triple-grating spectrometer (Princeton Instruments, Trivista 555) equipped with a liquid N_2-cooled, UV-enhanced CCD detector. Prior to the measurement, samples were calcined at 300 °C for 4 h. In situ Raman spectra were collected at room temperature with flowing He in the fluidized bed reactor described previously.[11]

Infrared Spectroscopy of Adsorbed Pyridine. For pyridine adsorption experiments, catalysts were preheated at 200 °C under vacuum (<5 mTorr) and cooled to room temperature. Then pyridine was injected through a septum using a syringe onto the catalysts under vacuum at room temperature. Subsequently, the catalysts were heated at 200 °C for 1 h under vacuum to remove physisorbed pyridine. The adsorbed catalysts were cooled to RT and mounted in an infrared cell having CaF_2 windows. Nitrogen gas was used to purge the sample chamber as well as the spectrometer. The FTIR spectra were recorded using a Nicolet Nexus 670 FTIR spectrometer coupled to an MCT detector with 2 cm^{-1} resolution.

Density Functional Theory Computational Methods. First-principles calculations based on the hybrid density functional theory (B3LYP)[12] have been performed to understand the binding of Zn on silica surface as well as the catalytic mechanism of propane dehydrogenation and propylene hydrogenation. The surface is represented using a cluster model consisting of different size siloxane rings (silsesquioxane),[13] which has been shown to be good approximations of local sites on amorphous silica surfaces. The electronic effect on amorphous silica is mostly local; therefore, cluster models are reasonably accurate for studying chemical reactions. The structure optimizations and free energy calculations of different reaction intermediates and transition states are performed using the Gaussian-09 quantum chemistry software.[14] The accuracy of the transition state (TS) calculations was verified by performing the intrinsic reaction coordinate (IRC) scan[15] and frequency analysis. TZVP basis sets[16] were used to perform all the calculations (B3LYP/TZVP).

3. RESULTS AND DISCUSSION

The Zn-on-silica catalyst was prepared by the method of strong electrostatic adsorption.[8] The hydroxyl groups on SiO_2 are weakly acidic with a point of zero charge, or isoelectric point, of pH 4. Thus, in basic aqueous solution, the hydroxyl groups are deprotonated, resulting in a negatively charged support surface. Because of the strong Coulombic attraction between the support and the Zn cation precursor, addition of the tetraaminezinc(II) nitrate solution gives an equilibrium zinc coverage of ~1.2 Zn^{2+}/nm^2. The amine ligands are subsequently removed by the subsequent thermal treatment to give 3.9% Zn on SiO_2 by weight on the high-surface-area silica.

Catalytic Performance: Propylene Hydrogenation and Propane Dehydrogenation. Catalytic rates of propane dehydrogenation and propylene hydrogenation on the silica-supported Zn catalysts are presented in Table 1. The turnover frequency (TOF) is based on the total amount of Zn. Figure 1 shows the rate and selectivity for propane dehydrogenation with the time on stream for Zn/SiO_2 and SiO_2 (no Zn). The rate and low selectivity of silica is identical to that of an empty tube, that is, gas-phase thermal cracking.[17]

Table 1. Turnover Frequencies for Propylene Hydrogenation at 200 °C and Propane Dehydrogenation at 550 and 650 °C for the Zn/SiO_2 Catalyst

t (h)	TOF (h^{-1})	r/r_0
	Hydrogenation	
0	0.303	0.974
12	0.295	
	Dehydrogenation	
0 (550 °C)	0.772	0.511
12 (550 °C)	0.394	
0.5 (650 °C)	2.3[a]	n/a

[a]Catalytic propene selectivity >95%.

The Zn/SiO_2 displays catalytic hydrogenation activity at temperatures above about 150 °C. The results presented in Table 1 for propylene hydrogenation at 200 °C were determined under differential conversion of 8.2%. Under these conditions, the SiO_2 support is unreactive. During the 16-h test period, there is little deactivation, as the steady-state conversion after 12 h is 97% that of the initial conversion. No products other than propane were observed. Few zinc materials, homogeneous or heterogeneous, have been observed to catalytically or even stoichiometrically hydrogenate or otherwise react with olefins. Stoichiometric 1,2-Zn−H addition across an olefin is rare, but it has been shown that Zn−H adds across an olefin in a stoichiometric reaction with a Ti[18] or Ni[19] complex present. Zn/ZSM-5 has not been shown to be active for olefin hydrogenation because olefins are rapidly polymerized over the protons in the catalyst framework. The fact that Zn/SiO_2 requires elevated reaction temperatures for hydrogenation catalysis is consistent with the difficulty expected for insertion of an olefin into a Zn−H and the stability of zinc alkyls toward the microscopic reverse reaction, β-hydride

dx.doi.org/10.1021/cs401116p | ACS Catal. 2014, 4, 1091−1098

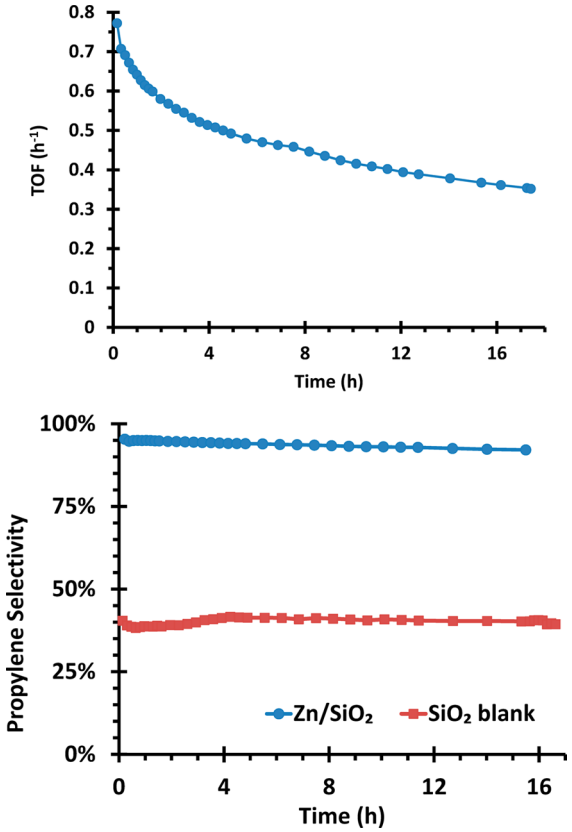

Figure 1. (a) The turnover frequency (TOF) per hour of catalyst for dehydrogenation of propane at 550 °C and (b) the selectivity to propylene; blue circles, Zn/SiO_2; red squares, SiO_2 blank (thermal cracking).

elimination. However, because hydrogenation catalysis is well-behaved, we surmised that Zn/SiO_2 might catalyze alkane dehydrogenation.

The thermal stability of Zn/SiO_2 allows it to be employed as an alkane dehydrogenation catalyst at temperatures where the reaction becomes thermodynamically favorable (T > ~550 °C). Above ~600 °C, thermal cracking (tested both in an empty tube and with SiO_2) is significant, resulting in products from both C−H bond breaking (propylene and hydrogen) and C−C bond breaking (methane and ethylene). The selectivity of gas-phase cracking is ~4:3 C−H bond breaking products to C−C bond breaking products (i.e., selectivies of 40%, 30%, and 30% propylene, methane, and ethylene, respectively), consistent with what has been reported in the literature.[17] At 550 °C, gas-phase thermal cracking is small, and the Zn/SiO_2 catalyst exhibits >95% selectivity to propylene and hydrogen throughout the course of the reaction. Furthermore, the catalyst is active for several hours, with the rate decreasing to ~50% of the initial conversion after 12 h. In this experiment, propane conversion ranged from 5 to 20% and was intentionally kept low to perform accurate kinetics under differential conditions (the equilibrium conversion at 550 °C is ~37%[2]). The selectivity of Zn/SiO_2 dehydrogenation selectivity was similarly high at higher propane conversions. At 650 °C, where significant contribution from thermal cracking was observed, the catalytic dehydrogenation selectivity remained high at 95% propylene.

Catalyst Structure: X-ray Absorption and Raman Spectroscopy. The oxidation state and coordination geometry of the active site was investigated using in situ X-ray absorption spectroscopy. X-ray absorption near edge structure (XANES) edge energies, presented in Table 2 and Figure 2a,c,

Table 2. Zn K-edge EXAFS and XANES Fits of the Zn/SiO_2 Catalyst

treatment[a]	edge energy, keV	N_{Zn-O}	R, Å	$\Delta\sigma^2$, ×10^3	E_0, eV
as prepared, RT	9.6630	4.0	1.95	1.0	−1.6
He 200 °C, He RT	9.6630	3.7	1.94	1.0	−1.7
H_2 200 °C, H_2 RT	9.6630	3.7	1.94	1.0	−1.7
H_2 + C_3H_6 200 °C, He RT	9.6630	3.7	1.94	1.0	−1.8
450 °C He, He RT	9.6626	3.1	1.93	1.0	−1.6
C_3H_8 550 °C, He RT	9.6626	3.1	1.93	1.0	−1.7
C_3H_8 550 °C	9.6626	2.9	1.92	6.0	−3.0
	References				
ZnO	9.6623	4.0	1.98	0.0	−0.3
Zn acetate (Zn^{2+} standard)	9.6646				
Zn foil (Zn^0 standard)	9.6590				

[a]RT = room temperature.

were recorded under the reaction conditions and at lower temperature after reaction. The XANES energy of the catalyst is similar to the reference compounds of ZnO and Zn acetate, consistent with Zn(II) ions. Furthermore, over a range of conditions, the XANES shape (figure 2c) and edge energies (Table 2) remain unchanged, suggesting that the Zn oxidation state does not change during reaction. These results differ from those reported for Zn/ZSM-5 catalysts. For example, in the study by Biscardi et al.,[20] although there was no shift in the edge energy, there was a significant change in the shape of the XANES edge when the temperature increased above 50 °C; the shape continued to change up to 300 °C. Because H_2O pulses restored the shape, it was concluded that this shape change was due to H_2O desorption. For Zn/silica, there is no change in the XANES at low temperature, which is indicative of H_2O desorption, as observed for Zn/MFI.

In addition to the EXAFS spectra obtained under reaction conditions, Zn coordination geometry was more reliable for data obtained after cooling to lower temperature because of the uncertainty in the fit parameter at high temperatures. Thus, EXAFS was obtained both at reaction temperature and after cooling to room temperature. The EXAFS fit results for the first shell Zn−O coordination are also given in Table 2. For the as-prepared catalyst, there are four Zn−O bonds at 1.94 Å, slightly shorter than those in bulk ZnO, (see the first shell peak in Figure 2b). Although there is a slight change in the coordination number after heat treatments at 200 °C, a significant change does not occur until the catalyst is heated to 450 °C. At elevated temperature, the Zn−O coordination number decreases from 4 to 3, accompanied by only a minor decrease in the Zn−O bond distance. In Figure 3c, the higher shell peak at ~2.4 Å (phase-uncorrected distance) is very small, suggesting little if any formation of Zn−O−Zn bonds. Even after heating at temperatures up to 700 °C, there is no observable increase in the size of the higher shell peaks, indicating high thermal stability of the surface structure. Again, these observations are different from those reported in the literature for Zn/ZSM-5. Biscardi et al.[20] observed that a fresh sample of Zn/ZSM-5 had a Zn−O coordination number of 5.4 at a distance of 2.09 Å. When heated to 500 °C, the

dx.doi.org/10.1021/cs401116p | ACS Catal. 2014, 4, 1091−1098

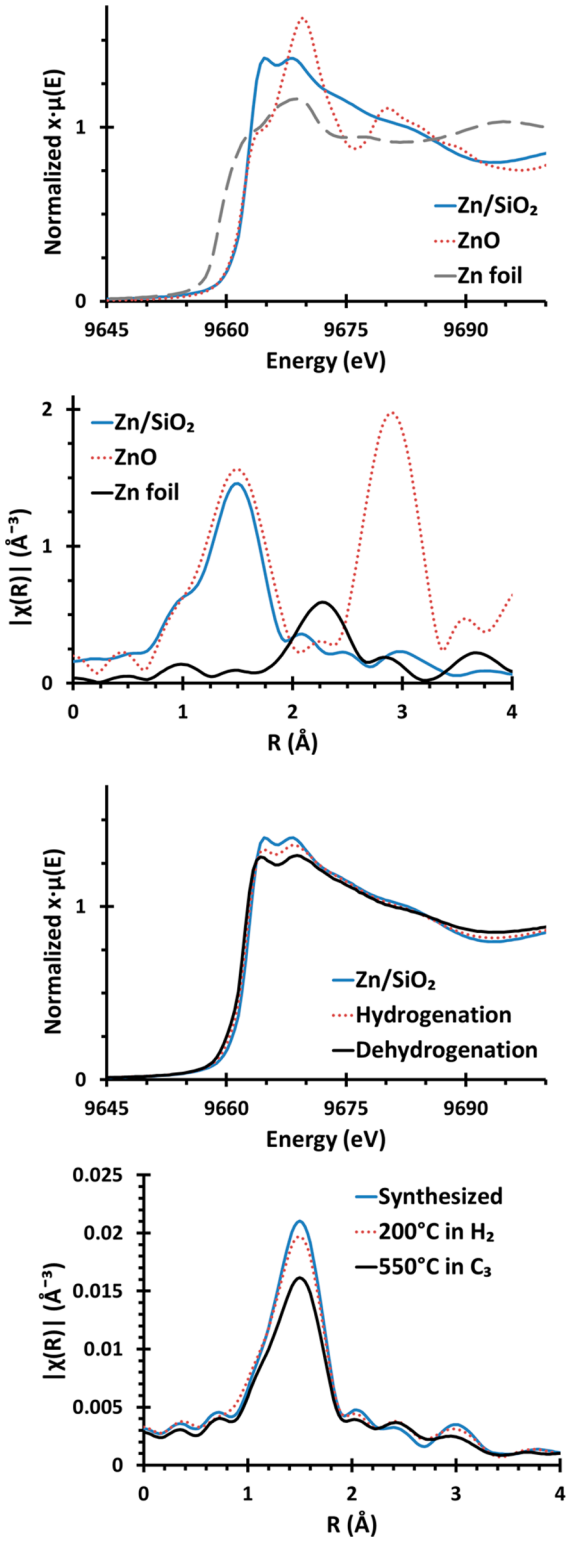

Figure 2. X-ray absorption spectroscopy analysis of the Zn/SiO_2 catalyst. (a) XANES; (b) Fourier transform magnitudes of EXAFS; (c) in situ XANES spectra for Zn/SiO_2 catalyst at room temperature in He, under hydrogenation conditions (in H_2 and propylene at 200 °C), and under dehydrogenation conditions (in propane at 550 °C); and (d) in situ EXAFS spectra for Zn/SiO_2 catalyst at room temperature in He, under propylene hydrogenation at 200 °C, and under dehydrogenation conditions (in propane at 550 °C).

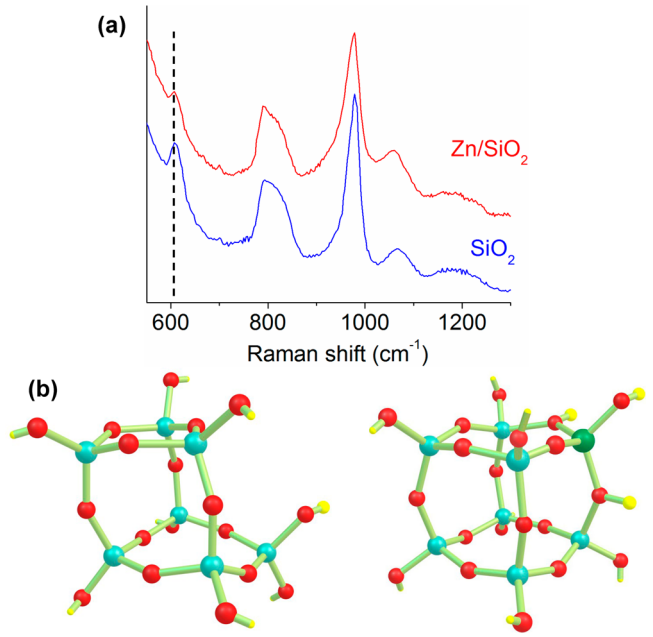

Figure 3. (a) In situ UV-resonance Raman spectra obtained in helium flow of SiO_2 and Zn/SiO_2 after calcination at 300 °C. The dashed line at 608 cm^{-1} represents the O-breathing mode in 3-membered siloxane rings on silica. (b) DFT-optimized cluster models showing 3-membered siloxane rings on silica before and after Zn incorporation. The calculations predict that Zn is tetracoordinated at room temperature but become three-coordinated under catalytic conditions. Color: Si (blue), O (red), H (yellow), and Zn (green).

coordination number dropped to 4.1, which corresponds to the water loss detected in the XANES spectra; however, at high temperatures, there is not further loss to 3 coordinate Zn−O as observed on Zn/SiO_2.

The Zn coordination to the silica surface was also studied by in situ UV Raman. Spectra of silica (no Zn) and the Zn/SiO_2 catalyst are shown in Figure 3a; the peak assignments from 600 to 1400 cm^{-1} are given in Table 3 along with their DFT

Table 3. Vibrational Frequencies of the Raman Bands of SiO_2, the DFT Calculated Frequencies, and Assignments

Raman (cm^{-1})	DFT (cm^{-1})	assignments[21a,22]
450	458	5-/6-membered $(SiO)_x$ rings in silica network
490	490	4-membered siloxane rings, defect 1 (D1)
608	604	3-membered siloxane rings, defect 2 (D2)
796, 824	802−843	symmetric Si−O−Si
978	948	Si−OH stretching
1068	1036−1043	asymmetric Si−O−Si, transverse mode (perpendicular to the direction of periodicity)
~1200	1135−1140	asymmetric Si−O−Si, longitudinal mode (parallel to the direction of periodicity)

calculated vibrational frequencies and structure. In silica, prominent Raman peaks emanate from defect sites in the form of siloxane rings (i.e., $(SiO)_x$ rings; see Figure 3b for an example of a $(SiO)_3$ defect ring). There is an increase in the vibrational frequency from 450, 490, and 608 cm^{-1} as the size of siloxane rings decreases from 5- or 6- to 4- and then 3-membered rings.[21] In Figure 3a, there is a peak at ~608 cm^{-1} on the silica support, evidencing the 3-membered siloxane rings, which significantly decreases in intensity upon addition of

dx.doi.org/10.1021/cs401116p | ACS Catal. 2014, 4, 1091−1098

Zn ions. By contrast, the other bands of the other siloxane ring are largely unchanged. During impregnation, the Zn cation inserts into the 3-membered Si−O ring to form a more stable 4-membered ring. A proposed structure of the $(SiO)_3$ defect ring and a tetrahedrally coordinated, single-site Zn in the defect site is shown in Figure 3b. This structure is consistent with the calculated stable binding of tetrahedral zinc in the corner vacancy of the SiO_2 (vide infra).

The Zn(II) surface site in silica differs from that of ion exchanged cations in MFI. For example, Zn ions in silica have three Zn−O−Si covalent bonds, whereas in zeolites, the cation is ionically bonded to the negatively charged Si−O−Al surface site. As a result of the ionic bonding in zeolites, the Zn(II) ion can adsorb H_2O at low temperature, forming $Zn(H_2O)_6^{2+}$, but similar hydration of the Zn(II) on silica does not occur.

Infrared Spectroscopy of Adsorbed Pyridine and Lewis Base Adsorption. Similar to Zn in ZSM-5,[23] Zn ions on silica readily adsorb pyridine. Strong infrared bands at 1612 and 1452 cm^{-1} and a smaller band at 1493 cm^{-1} are consistent with pyridine adsorbed on Lewis acid sites, and no bands were observed that were indicative of adsorption on Brönsted sites. In the absence of Zn ions, silica does not adsorb pyridine at 200 °C.

For organic reactions, often Lewis acid catalysts are highly sensitive to traces of water and other strongly coordinating solvents.[24] Because Zn(II) ions are Lewis acids, controlled poisoning by Lewis bases (isopropyl alcohol and pyridine) were used to determine the number of catalytically active sites. Figure 4 shows the relative decrease in the normalized rate (i.e.,

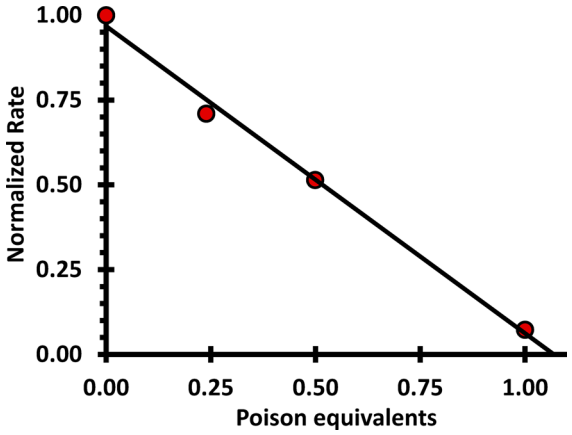

Figure 4. Effect of 2-propanol (0.25 and 0.5 equiv) and pyridine (1.0 equiv) poisoning on the hydrogenation rate by Zn/SiO_2.

1 = 0.303 h^{-1}) as a function of poison equivalents. There is a linear decrease in the normalized rate per equivalent of added poison. More importantly, the slope of the line indicates that there is a 1:1 stoichiometry between the poison and the hydrogenation rate, suggesting that every Zn is active, with equivalent rate. Finally, FT-IR spectroscopy showed that bound pyridine remained on the Zn/SiO_2 after performing a 1:1 poisoning experiment in which propene hydrogenation was indistinguishable from background SiO_2. For Zn/ZSM-5, both isolated Zn atoms or diatomic $[ZnOZn]^{2+}$ clusters have been proposed as active sites. The poisoning stoichiometry in the Zn/SiO_2 catalyst is consistent with isolated Zn ions, rather than Zn dimers, which would give a poisoning stoichiometry of 0.5 equiv per Zn.

Density Functional Theory: The Reaction Pathway and Activation Energies. On the basis of the structure of the Zn/SiO_2 catalysts deduced from the characterizations, DFT calculations for potential reaction pathways and reaction intermediates were performed and are summarized schematically in Figure 5. Although the as-synthesized Zn is

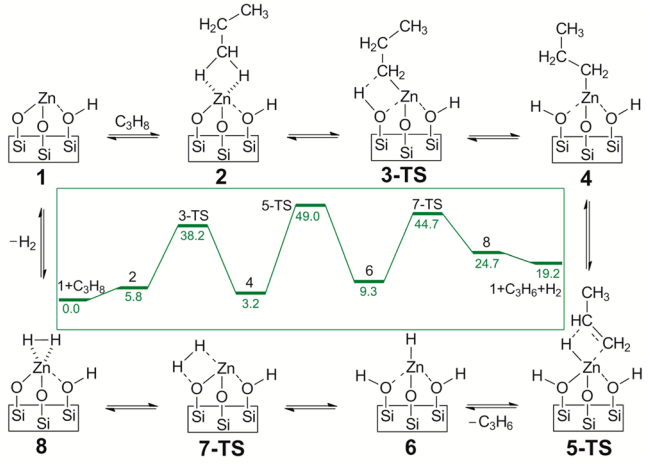

Figure 5. DFT calculated proposed catalytic reaction pathway for olefin hydrogenation and alkane dehydrogenation on single-site, Zn Lewis acid catalyst. The reaction free energies (kcal/mol) are shown in the inset.

tetrahedrally coordinated, under reaction conditions, there is loss of one coordinated oxygen, presumably as water, to form a 3-coordinate, Lewis acidic zinc. On the basis of this structure as a starting point for propane dehydrogenation, the C−H bond in propane is heterolytically cleaved to form a zinc alkyl (negative charge on the C) and bridging hydroxyl (proton from the C−H bond) group (intermediate 4), which is consistent with observations by Kokes, et al. of stoichiometric alkane activation by bulk ZnO.[25] This is also consistent with the "alkyl" mechanism proposed by van Santen.[26] The resulting β-hydrogen transfer (5-TS) to form propene and a zinc hydride is the calculated rate-limiting step. In the Zn/ZSM-5 literature, this step is facilitated by the H^+ ion's absorbing to a distantly located $[AlO_2]^-$ site in the zeolite framework. Because there is no Al present in our catalyst, the Zn−O−Si site serves as the H^+ adsorption site. Zinc alkyls are known to be particularly resistant to β-hydride elimination; however, the catalysis temperature is well above the documented reaction for zinc alkyls.[27] A separately computed pathway for C−C cracking was found; however, the transition state for C−C cracking, which involved β-methyl transfer to Zn, is at least 10 kcal/mol higher in energy than β-H transfer for the dehydrogenation rate-limiting step. This is consistent with the observed high selectivity of Zn/SiO_2 for alkane dehydrogenation over C−C bond cleavage.

For the microscopic reverse olefin hydrogenation pathway, H_2 heterolytically reacts at the Zn Lewis acid, producing a Zn−H and SiOH. Olefin insertion occurs at the Zn−H bond from the gas phase, and proton transfer to the Zn-alkyl bond completes the catalytic cycle. The cycle proceeds without a change in the Zn oxidation state. In both reaction directions, the coordinatively unsaturated Lewis acid attacks a σ bond, C−H or H−H, rather than coordinating to a lone pair of electrons, as in typical Lewis acid catalyzed reactions. Electron-deficient

dx.doi.org/10.1021/cs401116p | ACS Catal. 2014, 4, 1091−1098

metal centers have been shown to interact with σ bonds by catalyzing a four-centered transition state in σ-bond metathesis, and the related σ-complex-assisted metathesis (σ-CAM) mechanism.[28] However, the proton is directly transferred from one ligand to another during the reaction. In these cases, the resulting reaction is degenerate scrambling of hydrogen between hydrocarbon and other ligands.

In addition, σ-bond metathesis and heterolytic splitting of C−H bonds has also been observed with metal hydroxides[29,30] and across metal−carbon multiple bonds.[31] Again, alkane exchange is the observed reaction performed by these species. Catalytically mediating a substrate transformation rather than degenerate exchange at the metal center remains a significant challenge for alkane activation. Lewis acidic Zn/SiO_2 demonstrates this ability, representing a distinct advantage over other, related catalysts. Finally, the strong Si−O bond prevents further reaction of the catalytic site to lose water, reduce the zinc site, to aggregate into nanoparticles, or to otherwise decompose under the high temperatures necessary for alkane dehydrogenation.

The reaction pathway proposed above is also reminiscent of that for the Brönsted acid (BA) catalyzed monomolecular cracking of alkanes at low conversion.[6,32] In zeolites, for example, the proton attacks C−C bonds and, to a lesser extent, C−H bonds. The reaction is thought to occur by a three-center-two-electron transition state with the reactive proton and an alkane σ bond.[33] The initial alkane activation transition state calculated and proposed as 3-TS in Figure 5 contains a similar polarization of the C−H σ bond, resulting in heterolytic cleavage to form the zinc alkyl.

There are a number of significant differences between the LA catalyzed reactions of alkanes and olefins to those of BA. First, the LA primarily activates alkane C−H bonds, whereas the BA reacts nearly statistically with C−C or C−H σ bonds. As a result, the primary reaction catalyzed by Zn/SiO_2 produces almost exclusively H_2 and olefin, whereas on zeolite catalysts, the C−C cleavage leads primarily to lower-molecular-weight alkanes in addition to olefins. Second, the Zn Lewis acid is unreactive with the olefin product, and olefins readily undergo secondary reactions in zeolites, such as oligomerization, skeletal isomerization, bimolecular cracking, aromatic formation, etc. Cleavages that produce methane are especially unproductive because BA catalysts cannot reincorporate it into the catalytic cycle. The low reactivity of olefin products with the LA means that the dehydrogenation selectivity is high at all conversions, but for BA alkane dehydrogenation, it is observed only at low conversions. Finally, although BA sites catalyze alkane dehydrogenation, albeit at low conversion, they have not been reported to catalyze olefin hydrogenation, unlike what is observed for the Zn/SiO_2 Lewis acid catalyst.

The olefin hydrogenation and alkane dehydrogenation reactions reported here are not unique to the Zn/SiO_2 catalyst. We have identified several other single-site Lewis acid catalysts that, like the Zn^{2+} ion, exist in a single oxidation state, are structurally and kinetically stable at high reaction temperatures, and have high selectivity for alkane dehydrogenation catalysis. These will be reported in the near future.

4. CONCLUSIONS

Zn(II) ions on SiO_2 react with 3-membered surface siloxane defects to form tetrahedrally coordinated single sites with 3 Si−O−Zn surface bonds. At elevated temperature, there is loss of one Zn−O bond, forming a coordinatively unsaturated, 3-coordinate Zn^{2+} catalytic site capable of olefin hydrogenation at temperatures near 200 °C and the microscopic reverse alkane dehydrogenation reaction at temperatures above about 550 °C. Under reaction conditions, the Lewis acid center Zn/SiO_2 does not undergo a change in the Zn oxidation state, but functions through the heterolytic cleavage pathway of H−H or C−H bonds as intermediates, where alkyl or hydride ligands are bonded to the Zn(II) and a proton is transferred to the support oxygen ion. The computed mechanism and energetics for C−C cleavage in alkanes is significantly higher than that for C−H dissociation explaining the high olefin selectivity for alkane dehydrogenation. Without Brønsted acid sites in the Zn/SiO_2 catalyst, the high propylene selectivity for propane dehydrogenation confirms the catalytic role of Zn ions in ZSM-5, which is often proposed during the catalytic conversion of alkanes to aromatics.

AUTHOR INFORMATION

Corresponding Authors

*E-mail: millerjt@anl.gov.

*E-mail: ahock@iit.edu.

Present Addresses

[⊥](N.M.S.) Northwestern University, Evanston, Illinois 60208, United States.

[‖](J.G.) Department of Chemical Engineering, Purdue University, West Lafayette, Indiana 47907, United States.

Notes

The authors declare no competing financial interest.

ACKNOWLEDGMENTS

The work at Argonne National Laboratory was supported by the U.S. Department of Energy, Office of Basic Energy Sciences, Chemical Sciences under Contract DE-AC-02-06CH11357. B.H. and A.S.H. thank the Illinois Institute of Technology for a Starr-Fieldhouse Fellowship (B.H.) and startup funding support. J.G. acknowledges support through a DOE Early Career Award of the Chemical Sciences Division, Office of Basic Energy Sciences, Office of Science, U.S. Department of Energy. Use of the Advanced Photon Source is supported by the U.S. Department of Energy, Office of Science, and Office of Basic Energy Sciences, under Contract DE-AC02-06CH11357. Materials Research Collaborative Access Team (MRCAT, Sector 10-BM) operations are supported by the Department of Energy and the MRCAT member institutions.

REFERENCES

(1) Ren, T.; Patel, M.; Blok, K. *Energy* **2006**, *31* (4), 425−451.

(2) Bhasin, M. M.; McCain, J. H.; Vora, B. V.; Imai, T.; Pujado, P. R. *Appl. Catal., A* **2001**, *221* (1−2), 397−419.

(3) (a) Dent, A. L.; Kokes, R. J. *J. Am. Chem. Soc.* **1969**, *91* (25), 7207−7208. (b) Dent, A. L.; Kokes, R. J. *J. Am. Chem. Soc.* **1970**, *92* (4), 1092−1093. (c) Dent, A. L.; Kokes, R. J. *J. Phys. Chem.* **1969**, *73* (11), 3772−3780. (d) Dent, A. L.; Kokes, R. J. *J. Phys. Chem.* **1969**, *73* (11), 3781−3790. (e) Dent, A. L.; Kokes, R. J. *J. Phys. Chem.* **1970**, *74* (20), 3653−3662. (f) Kokes, R. J. *Acc. Chem. Res.* **1973**, *6* (7), 226−233. (g) Conner, W. C.; Innes, R. A.; Kokes, R. J. *J. Am. Chem. Soc.* **1968**, *90* (24), 6858−6858.

(4) Greenwood, N. N.; Earnshaw, A. *Chemistry of the Elements*, 2nd ed.; Elsevier: Dordrecht, The Netherlands, 1997.

(5) (a) Biscardi, J. A.; Meitzner, G. D.; Iglesia, E. *J. Catal.* **1998**, *179* (1), 192−202. (b) Berndt, H.; Lietz, G.; Lücke, B.; Völter, J. *Appl. Catal., A* **1996**, *146* (2), 351−363.

(6) Kwak, B. S.; Sachtler, W. M. H.; Haag, W. O. *J. Catal.* **1994**, *149* (2), 465−473.
(7) Narbeshuber, T. F.; Brait, A.; Seshan, K.; Lercher, J. A. *J. Catal.* **1997**, *172* (1), 127−136.
(8) de Jong, K. P. *Synthesis of Solid Catalysts*. Wiley-VCH Verlag GmbH & Co. KGaA: Weinheim, 2009.
(9) Setthapun, W.; Williams, W. D.; Kim, S. M.; Feng, H.; Elam, J. W.; Rabuffetti, F. A.; Poeppelmeier, K. R.; Stair, P. C.; Stach, E. A.; Ribeiro, F. H.; Miller, J. T.; Marshall, C. L. *J. Phys. Chem. C* **2010**, *114* (21), 9758−9771.
(10) Abrahams, S. C.; Bernstein, J. L. *Acta Crystallogr., Sect. B* **1969**, *25*, 1233−1236.
(11) Kim, H.; Kosuda, K. M.; Van Duyne, R. P.; Stair, P. C. *Chem. Soc. Rev.* **2010**, *39* (12), 4820−4844.
(12) Becke, A. D. *J. Chem. Phys.* **1993**, *98* (7), 5648−5652.
(13) Feher, F. J.; Newman, D. A.; Walzer, J. F. *J. Am. Chem. Soc.* **1989**, *111* (5), 1741−1748.
(14) Frisch, M. J.; Trucks, G. W.; Schlegel, H. B.; Scuseria, G. E.; Robb, M. A.; Cheeseman, J. R.; Scalmani, G.; Barone, V.; Mennucci, B.; Petersson, G. A.; Nakatsuji, H.; Caricato, M.; Li, X.; Hratchian, H. P.; Izmaylov, A. F.; Bloino, J.; Zheng, G.; Sonnenberg, J. L.; Hada, M.; Ehara, M.; Toyota, K.; Fukuda, R.; Hasegawa, J.; Ishida, M.; Nakajima, T.; Honda, Y.; Kitao, O.; Nakai, H.; Vreven, T.; Montgomery, J. A., Jr.; Peralta, J. E.; Ogliaro, F.; Bearpark, M.; Heyd, J. J.; Brothers, E.; Kudin, K. N.; Staroverov, V. N.; Kobayashi, R.; Normand, J.; Raghavachari, K.; Rendell, A.; Burant, J. C.; Iyengar, S. S.; Tomasi, J.; Cossi, M.; Rega, N.; Millam, N. J.; Klene, M.; Knox, J. E.; Cross, J. B.; Bakken, V.; Adamo, C.; Jaramillo, J.; Gomperts, R.; Stratmann, R. E.; Yazyev, O.; Austin, A. J.; Cammi, R.; Pomelli, C.; Ochterski, J. W.; Martin, R. L.; Morokuma, K.; Zakrzewski, V. G.; Voth, G. A.; Salvador, P.; Dannenberg, J. J.; Dapprich, S.; Daniels, A. D.; Farkas, Ö.; Foresman, J. V.; Ortiz, J. B.; Cioslowski, J.; Fox, D. J. *Gaussian 09, Revision D.01*; Gaussian Inc.: Wallingford, CT, 2009.
(15) Hratchian, H. P.; Schlegel, H. B. *J. Chem. Theory Comput.* **2005**, *1* (1), 61−69.
(16) Schafer, A.; Huber, C.; Ahlrichs, R. *J. Chem. Phys.* **1994**, *100* (8), 5829−5835.
(17) Buekens, A. G.; Froment, G. F. *Ind. Eng. Chem. Proc. Des. Dev.* **1968**, *7* (3), 435−447.
(18) Gao, Y.; Urabe, H.; Sato, F. *J. Org. Chem.* **1994**, *59* (19), 5521−5523.
(19) Vettel, S.; Vaupel, A.; Knochel, P. *Tetrahedron Lett.* **1995**, *36* (7), 1023−1026.
(20) Biscardi, J. A.; Meitzner, G. D.; Iglesia, E. *J. Catal.* **1998**, *179* (1), 192−202.
(21) (a) Humbert, B.; Burneau, A.; Gallas, J. P.; Lavalley, J. C. *J. Non-Cryst. Solids* **1992**, *143* (0), 75−83. (b) Morrow, B. A.; McFarlan, A. J. *J. Non-Cryst. Solids* **1990**, *120*, 61−71. (c) Brinker, C. J.; Brow, R. K.; Tallant, D. R. *J. Non-Cryst. Solids* **1990**, *120*, 26−33.
(22) (a) Galeener, F. L.; Mikkelsen, J. C., Jr. *Phys. Rev. B* **1981**, *23* (10), 5527−5530. (b) Borodko, Y.; Ager, J. W.; Marti, G. E.; Song, H.; Niesz, K.; Somorjai, G. A. *J. Phys. Chem. B* **2005**, *109* (37), 17386−17390.
(23) El-Malki, El-M.; van Santen, R. A.; Sachtler, W. M. H. *J. Phys. Chem. B* **1999**, *103*, 4611−4622.
(24) Panov, A. G.; Fripiat, J. J. *Catal. Lett.* **1999**, *57*, 25−32.
(25) Kokes, R. J. *Acc. Chem. Res.* **1973**, *6* (7), 226−233.
(26) Zhidomirov, G. M.; Shubin, A. A.; Kazansky, V. B.; van Santen, R. A. *Theor. Chem. Acc.* **2005**, *114*, 90−96.
(27) Koszinowski, K.; Müller, C.; Brand, H.; Fleckenstein, J. E. *Organometallics* **2012**, *31* (20), 7165−7170.
(28) Perutz, R. N.; Sabo-Etienne, S. *Angew. Chem., Int. Ed.* **2007**, *46* (15), 2578−2592.
(29) Ess, D. H.; Gunnoe, T. B.; Cundari, T. R.; Goddard, W. A.; Periana, R. A. *Organometallics* **2010**, *29* (24), 6801−6815.
(30) Foley, N. A.; Lail, M.; Lee, J. P.; Gunnoe, T. B.; Cundari, T. R.; Petersen, J. L. *J. Am. Chem. Soc.* **2007**, *129* (21), 6765−6781.
(31) (a) Cundari, T. R.; Klinckman, T. R.; Wolczanski, P. T. *J. Am. Chem. Soc.* **2002**, *124* (7), 1481−1487. (b) Bennett, J. L.; Wolczanski, P. T. *J. Am. Chem. Soc.* **1997**, *119* (44), 10696−10719. (c) Schaller, C. P.; Cummins, C. C.; Wolczanski, P. T. *J. Am. Chem. Soc.* **1996**, *118* (3), 591−611. (d) Cummins, C. C.; Schaller, C. P.; Van Duyne, G. D.; Wolczanski, P. T.; Chan, A. W. E.; Hoffmann, R. *J. Am. Chem. Soc.* **1991**, *113* (8), 2985−2994. (e) Pamplin, C. B.; Legzdins, P. *Acc. Chem. Res.* **2003**, *36* (4), 223−233.
(32) Babitz, S. M.; Williams, B. A.; Miller, J. T.; Snurr, R. Q.; Haag, W. O.; Kung, H. H. *Appl. Catal., A* **1999**, *179* (1−2), 71−86.
(33) (a) Kotrel, S.; Knozinger, H.; Gates, B. C. *Microporous Mesoporous Mater.* **2000**, *35*−*6*, 11−20. (b) Collins, S. J.; Omalley, P. J. *J. Catal.* **1995**, *153* (1), 94−99.